PERGAMON

Acta mater. 48 (2000) 1105–1114

Acta MATERIALIA

www.elsevier.com/locate/actamat

FIELD-DEPENDENT NEUTRON DEPOLARIZATION STUDY OF THE FERRITE FORMATION IN MEDIUM-CARBON STEELS

S. G. E. TE VELTHUIS[1, 2], N. H. VAN DIJK[1, 3]†, M. TH. REKVELDT[1], J. SIETSMA[2] and S. VAN DER ZWAAG[2]

[1]Interfaculty Reactor Institute, Delft University of Technology, Mekelweg 15, 2629 JB Delft, The Netherlands, [2]Laboratory for Materials Science, Delft University of Technology, Rotterdamseweg 137, 2628 AL Delft, The Netherlands and [3]Netherlands Institute for Metals Research, Rotterdamseweg 137, 2628 AL Delft, The Netherlands

(Received 8 August 1999; accepted 20 October 1999)

Abstract—Neutron depolarization experiments have been performed on the ferrite and pearlite phase transformations of the medium-carbon C60 and C35 steels. The interaction of the polarized neutron beam with the ferromagnetic ferrite grains gives information on the mean magnetization and the magnetic correlation length. From these parameters the ferrite fraction and the mean ferrite grain size are determined *in situ* as a function of time and temperature during the phase transformations. The applied magnetic field was varied periodically in order to record a full hysteresis curve of the magnetization, which gives essential information on the microstructure of the ferromagnetic ferrite grains. The field dependence of the mean particle size during the early stages of the pearlite formation is a strong indication of multi-domain behavior, which is absent in the austenite–ferrite transformation and at the end of the pearlite formation. © *2000 Acta Metallurgica Inc. Published by Elsevier Science Ltd. All rights reserved.*

Keywords: Neutron depolarization; Steel; Phase transformations; Microstructure

1. INTRODUCTION

The austenite–ferrite phase transformation plays an important role in the evolution of the microstructure of carbon–manganese and related steels, and therefore, is an important step in the production process of hot-rolled steel strips. The kinetics of the phase transformation are usually studied by techniques such as dilatometry, differential scanning calorimetry and optical or electron microscopy. From dilatometry and differential scanning calorimetry, only information on the total fraction transformed can be acquired. From optical and electron microscopy, information on the grain size and morphology can be obtained. These latter methods, however, require the interruption of the transformation process, and only give information on a small amount of the material. In contrast, neutron depolarization measurements are sensitive to both the fraction transformed and the average morphology of the ferrite grains. These parameters are derived from the rotation and shortening of the polarization vector of a polarized neutron beam during transmission through a sample. The method has successfully been applied to study the phase transformations in several medium-carbon steels [1–4]. A major limitation of the use of neutron depolarization to study phase transformations in steel is that the transformation product must be ferromagnetic at all stages of the transformation. Since the Curie temperature T_C of ferrite is 1043 K, the phase transformations can only be studied below this temperature.

In this paper we concentrate on the formation of ferrite and pearlite in two medium-carbon steels: C35 and C60. Previous neutron depolarization measurements [1–4] were performed in a constant applied magnetic field and analyzed by assuming the magnetization alignment of the ferromagnetic phase along the applied magnetic field did not change during the transformation. The magnetization alignment of the ferromagnetic phase is an essential parameter in the determination of the ferrite fraction and the ferrite grain size, and was chosen in accordance with the equilibrium ferrite fraction at the end of the transformation. In the present experiment we have measured the magnetization alignment of the ferromagnetic phase by

† To whom all correspondence should be addressed.

1359-6454/00/$20.00 © 2000 Acta Metallurgica Inc. Published by Elsevier Science Ltd. All rights reserved.
PII: S1359-6454(99)00414-0

varying the applied magnetic field in order to measure a full hysteresis curve of the magnetization at each measuring point during the transformation. In the following, we will first describe the experimental method. Subsequently, the neutron depolarization measurements of a three-step isothermal transformation experiment on C60 steel and of a continuous cooling experiment on C35 steel are discussed. Finally, the experimental results are summarized.

2. NEUTRON DEPOLARIZATION

Neutron depolarization makes use of the interaction between the spin of a neutron and the local magnetic induction in a sample. The change in polarization of a polarized neutron beam upon transmission through a magnetic sample is generally described by [5, 6]

$$\mathbf{P}' = \mathbf{D}\mathbf{P}_0 \tag{1}$$

where $\mathbf{P}_0$ is the initial polarization vector, $\mathbf{P}'$ is the polarization vector after transmission, and $\mathbf{D}$ is the (3×3) depolarization matrix. The local magnetic induction in the sample $\mathbf{B}(\mathbf{r}) = \langle \mathbf{B} \rangle + \Delta\mathbf{B}(\mathbf{r})$ can be described by a sum of the mean magnetic induction $\langle \mathbf{B} \rangle$ and the local fluctuation of the magnetic induction $\Delta\mathbf{B}(\mathbf{r})$, with $\mathbf{r}$ indicating the position within the sample. The polarization vector is influenced by each of these two components in a different way. The mean magnetic induction will result in a rotation of the polarization vector around the mean magnetic induction vector $\langle \mathbf{B} \rangle$ by a rotation angle φ given by [7]

$$\varphi = (\gamma/v)L\langle B \rangle = (\gamma/v)Lfm\mu_0 M_s \tag{2}$$

where $\gamma = 1.83 \times 10^8$/s T is the gyromagnetic ratio, v is the velocity of the neutrons, and L is the transmission length of the sample. The mean magnetic induction of a ferromagnet is the product of the fraction of ferromagnetic material (ferrite) f, the reduced magnetization m and the spontaneous magnetic induction $\mu_0 M_s$. The reduced magnetization m quantifies the degree of magnetization alignment in the ferromagnetic phase. In the case of α-Fe, ferromagnetism occurs below the Curie temperature of $T_C = 1043$ K. The temperature-dependent saturation magnetization $M_s(T)$ of α-Fe has been measured in the vicinity of T_C by Stüsser and co-workers [8], who described the saturation magnetization by

$$M_s(T) = M_0 \tau^{\beta}\{1 + a\tau^{\Delta}\} \tag{3}$$

where $\tau = (T_C - T)/T_C$ is the reduced temperature. The constants $\mu_0 M_0 = 3.408$ T, $\beta = 0.365$, $a = -0.529$ and $\Delta = 0.55$, which will be used for the present experiments, have been determined by neutron depolarization experiments on pure polycrystalline Fe in the temperature range from 800 to 1050 K [9].

The local fluctuations $\Delta\mathbf{B}(\mathbf{r})$ will result in a shortening of the polarization vector (depolarization) by an amount proportional to the correlation function ξ of $(\Delta B)^2$ along the neutron path. This correlation function ξ is a measure of the mean ferrite particle size δ. If the magnetic field is applied along the y-axis (perpendicular to the transmission direction of the neutron beam) and the ferrite grains are assumed to be homogeneously distributed identical spheres, the mean particle size δ is related to ξ by [7, 10]

$$\delta = 3c_3\xi/\{2f(\mu_0 M_s)^2(1 - c_2 c_3 m^2)\} \tag{4}$$

where $c_2 = (4\pi f^{\,2}/81)^{1/3}$ and $c_3 = 32/(27 - 9\langle n_y^2 \rangle)$. Here $\langle n_y^2 \rangle$ is the average of the square of the reduced local magnetization and describes the anisotropy of the local magnetic fluctuations.

The rotation φ and the magnetic correlation function ξ can be expressed in terms of the depolarization matrix $\mathbf{D}$ by [7, 10]

$$\varphi = \arctan\{(D_{xz} - D_{zx})/(D_{xx} + D_{zz})\} \tag{5}$$

$$\xi = -\ln(\det \mathbf{D})/\{2L(\gamma/v)\}. \tag{6}$$

In order to obtain a direct relationship between the measured depolarization matrix $\mathbf{D}$ and the parameters of interest, the ferrite fraction f and the mean ferrite grain size δ, all the other parameters should be determined experimentally. The magnitude of m during all stages of the transformation can be established by varying the applied magnetic field during the measurement. The approach to saturation of the magnetization can be used to get an indication of m at the maximum applied magnetic field.

3. ISOTHERMAL EXPERIMENTS ON C60 STEEL

3.1. Experiment

We have performed neutron depolarization experiments on the isothermal transformation of C60 steel. The experiments were performed using a fixed neutron wavelength of 1.6 Å. The composition of the C60 steel sample, as determined by infrared absorption spectrometry and X-ray fluorescence, is given in Table 1. The equilibrium transformation temperatures for the C60 steel sample were evaluated with the multicomponent thermodynamic software program MTDATA®, and amount to $A_3 = 1010$ K for the austenite–ferrite transformation, $A_1^+ = 998$ K and $A_1^- = 973$ K for the pearlite formation. A ring-shaped sample, polished to a thickness of 0.33 mm, was placed in a slow-cooling furnace. After annealing the sample at 1073 K, the sample was cooled at a rate of 12 K/h to a tempera-

Table 1. Chemical compositions of the C60 and C35 steel samples. The C and S concentrations were measured using infrared absorption spectrometry and the concentration of the other elements was determined by X-ray fluorescence

Material	Elements (in wt%)									
	C	Mn	S	Si	P	Cr	Ni	Cu	Mo	Sn
C60	0.66	0.69	0.03	0.30	0.01	0.19	0.09	0.17	0.02	0.01
C35	0.364	0.656	0.021	0.305	0.014	0.177	0.092	0.226	0.016	0.017

ture just below the A_1^+-temperature. After holding it for several hours at a constant temperature of 993 K, the temperature was decreased twice in steps of 5 K. Eventually the sample was cooled to room temperature. The temperature–time sequence of this three-step isothermal experiment is given in Fig. 1(a). The time $t = 0$ is defined as the moment that the cooling started after annealing at 1073 K.

A varying magnetic field between 1650 and −1650 A/m was applied perpendicular to the transmission direction of the neutron beam. The time dependence of the applied magnetic field was described by a "saw-toothed" function with a period of 0.1 s, which was divided into 100 time channels. In each time channel the full depolarization matrix was measured at a different magnetic field value. The measurement of each magnetization curve lasted approximately 15 min in order to obtain sufficient counting statistics.

The final microstructure of the sample after the experiment has been studied by optical microscopy. It can be concluded that due to the long annealing at temperatures just below the A_1^+ temperature, a significant amount of spheroidizing of cementite has taken place. Furthermore, the remaining pearlite has a relatively large lamella spacing (≈ 2 μm) due to the high temperature (small undercooling) at which it was formed. The non-lamellar ferrite regions have a radius of approximately 10 μm. The equilibrium ferrite fractions calculated by MTDATA® amount to 7% of pro-eutectoid ferrite and 88% at the end of the transformation, in qualitative agreement with the microscopy results.

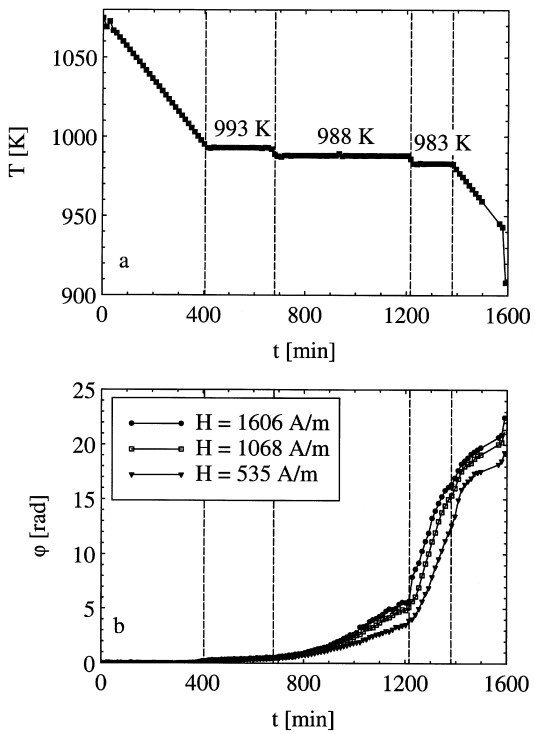

Fig. 1. The temperature profile (a) and the rotation of the polarization vector φ (b) for C60 steel as a function of time at different values of the applied magnetic field H. The vertical lines distinguish five different temperature regions.

3.2. Results

The determined rotation φ as a function of time for three different values of the applied field is given in Fig. 1(b). The transformation from austenite to ferrite starts during cooling at $t = 374$ min and $T = 1000$ K. The pearlite formation starts at the beginning of the second temperature step (at $t = 679$ min and $T = 988$ K), indicated by a gradual increase in $\mathrm{d}\varphi/\mathrm{d}t$. A sharp increase in the rotation is observed at the third temperature step (at $t = 1215$ min and $T = 983$ K). For each data point in Fig. 1(b) the field dependence of the rotation angle φ is measured. For six stages during the transformation, the field-dependent rotation φ of the polarization vector is given in Fig. 2. Since the variation in φ in a varying magnetic field only depends on the reduced magnetization m [equation (2)], these graphs are representative for the magnetization curves. It is obvious that the magnetic behavior changes during the transformation. First, the approach to saturation changes. At the beginning and at the end of the transformation ($t = 413$ and 1590 min), φ hardly changes with the field at high field values. This suggests that at these fields the magnetic structure is close to magnetic saturation. However, at intermediate transformation times there is a strong field dependence of φ, even at the highest field applied. Secondly, all the curves show magnetic hysteresis, with the coercive field becoming larger towards the end of the transformation.

In general, magnetic hysteresis can be caused by (1) the interactions between the local magnetization of a domain and the bulk magnetization, (2) domain wall pinning at grain boundaries or other inhomogeneities, (3) crystalline and shape anisotropy, and (4) demagnetization fields [11, 12]. The

relative importance of these effects is determined by the temperature and the microstructure. The crystalline anisotropy varies with temperature, but is relatively small at the temperature range of the present neutron depolarization experiments [13], limiting its influence on the magnetization. The proeutectoid ferrite grains formed at the beginning of the phase transformation are assumed to be single magnetic domains and because of the low fractions (large average distance between grains), the magnetic interactions between separate domains or grains are expected to be small. Therefore, shape anisotropy, demagnetization fields, and possibly to some extent pinning at the grain boundary will be the main factors that determine the magnetic hysteresis in the first stages of the phase transformation. When pearlite forms, the pinning of domain walls will play a more significant role. Various studies [14–16] of the magnetic behavior of steel at room temperature have shown that cementite plates in pearlite can act as pinning sites, and in fact are strong pinning sites when the domain wall lies parallel to the cementite plate. However, it is possible (even energetically favorable) for domain walls to cross the cementite plates perpendicularly. In that case they will pin at changes in the lamella orientation or at pearlite–ferrite boundaries.

A quantitative analysis of each measured magnetization curve yields the coercive field as a function of time, as given in Fig. 3(a). Four ranges can be distinguished. The first range is from the start of the phase transformation to about $t = 700$ min, where $H_c \approx 38$ A/m. At $t = 700$ min H_c slightly increases and then remains constant at $H_c \approx 43$ A/m until $t = 1200$ min. This increase in the coercive field can be explained by the formation of pearlite, which introduces pinning sites as explained above. The increase in H_c coincides with an increase in the rate at which the rotation φ changes [Fig. 1(b)], which also indicated the formation of pearlite. Between $t = 1200$ and 1350 min H_c increases rapidly from 43 to 86 A/m. This range roughly coincides with the range in which the temperature was held constant at 983 K, during which the rotation strongly increases, suggesting that the rest of the pearlite formation is taking place. Additional pinning sites due to the increase in the fraction of pearlite, as well as an increased interaction between magnetic domains due to a higher ferrite fraction, result in this strong increase in H_c. After $t = 1350$ min, during cooling to room temperature, the coercive field remains constant.

Since between $t = 1200$ and 1350 min the fraction of pearlite clearly influences H_c, it is unexpected that between $t = 700$ and 1200 min H_c changes very little. This might be understood in terms of the following considerations. Studies of the magnetic

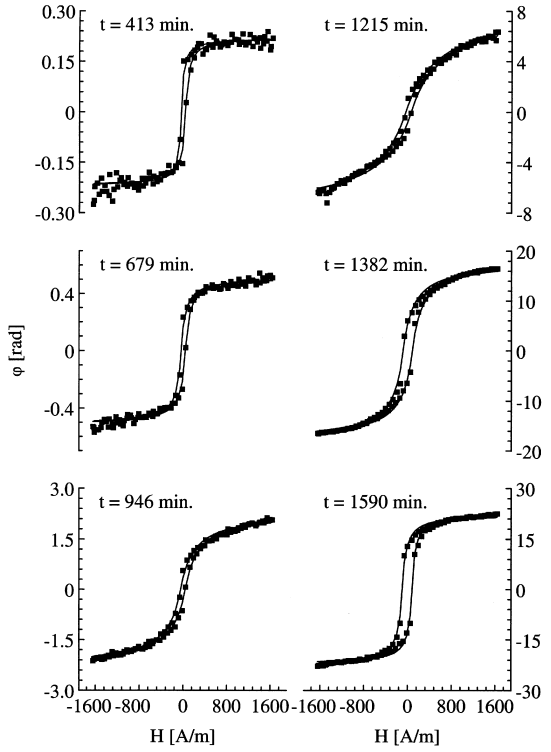

Fig. 2. The rotation of the polarization vector φ for C60 steel as a function of the applied magnetic field at different stages during the transformation. The data points are the measurements while the solid lines are the results of the fit with equation (7).

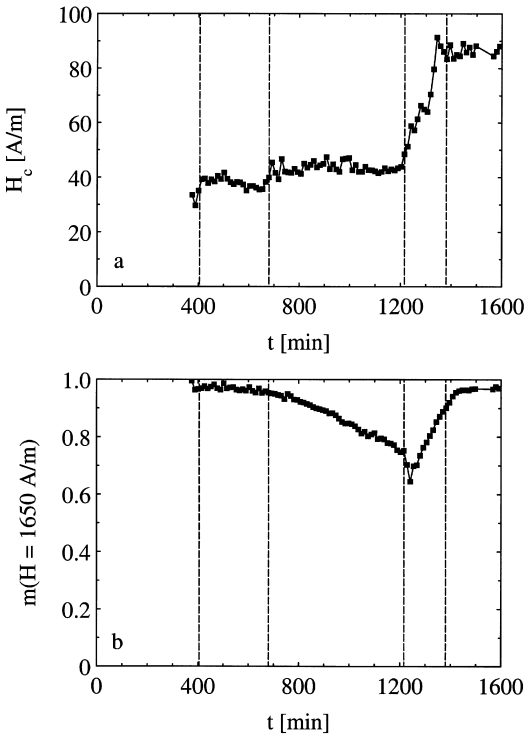

Fig. 3. The coercive field H_c (a) and the reduced magnetization at the highest applied field $m(H = 1650$ A/m) (b) for C60 steel as a function of time, determined by fitting the magnetization curves with equation (7).

behavior of pearlitic steels at room temperature [16–19] show that spheroidizing of cementite in pearlite reduces H_c, while regularly spaced pearlite with a small lamella spacing gives rise to a high H_c. The final microstructure of the sample after the experiment shows regions in which the lamellae are more or less regularly spaced, and other regions in which the structure is not regular and clearly a large degree of spheroidizing of the cementite has taken place. The pearlite that contains spheroidized cementite will have formed at the higher temperature, and due to its microstructure will have a smaller influence on H_c than pearlite formed at lower temperatures with a regular lamellar structure. In the case of the irregular pearlite structure, the pearlite–ferrite grain boundaries are less sharp, also limiting the influence of the formed pearlite on H_c.

From Fig. 2 it is clear that at the highest applied magnetic field the reduced magnetization is not constant throughout the transformation. In order to determine the field-dependent reduced magnetization $m(H)$ for each of the measured curves, it is necessary to know the saturation rotation φ_s, since $m(H) = \varphi(H)/\varphi_s$. As mentioned before, the value $m(H)$ is essential for the determination of the ferrite fraction f and the mean grain radius δ from the depolarization matrix measured at a magnetic field H. Therefore, we will determine φ_s from the measured magnetization curves $\varphi(H)$.

In the literature different approaches have been suggested to describe the magnetization curve [11]. These approaches take into account one or more of the effects on the magnetic hysteresis, such as the influence of anisotropy and the interaction between single-domain grains [20]. For the present measurements, the simple empirical equation for an anhysteretic magnetization curve derived by Frölich [21] and later by Kennelly [22] is used:

$$M = M_s/(1 + b/H_{eff}) \tag{7}$$

where M_s is the saturation magnetization, which is equal to the spontaneous magnetization, b is a constant depending on the microstructure, and H_{eff} is the effective magnetic field inside the sample. Hysteresis in the magnetization can be taken into account by defining $H_{eff} = H \pm H_c$, where H is the applied magnetic field outside the sample and H_c the coercive field, and the $+$ or $-$ sign refers to a decreasing or increasing applied magnetic field, respectively [23].

For the magnetization curves of Fig. 2, fits to the experimental data have been performed with equation (7) and the coercive field H_c of Fig. 3(a). As shown in Fig. 2, equation (7) can reasonably well describe the measured magnetization curves throughout the transformation. The reduced magnetization as a function of the applied magnetic field $m(H)$ corresponds to

$$m(H) = M(H)/M_s = \varphi(H)/\varphi_s = 1/\{1 + b/(H \pm H_c)\}. \tag{8}$$

The reduced magnetization at the highest applied field $m(H = 1650\ \mathrm{A/m})$ has been deduced from the fitting parameter b and is shown in Fig. 3(b). At the beginning and at the end of the transformation $m(H = 1650\ \mathrm{A/m})$ reaches a value of 0.96. Between $t = 700$ and 1240 min $m(H = 1650\ \mathrm{A/m})$ decreases to 0.64, indicating that when pearlite is being formed it is increasingly difficult to magnetically saturate the sample. Between $t = 1240$ and 1420 min the transformation comes to completion and the sample is filled with magnetic material, causing m to recede to the value that was found at the beginning of the transformation. Apparently, it becomes easier to align the magnetization along the applied magnetic field at higher ferrite fractions due to the interactions between the magnetic domains.

In principle, the ferrite fraction f can now be calculated from equation (2) using the determined $m(H)$ and the measured $\varphi(H)$. Using the values of $m(H)$ in Fig. 3(b), the ferrite fraction at the end of the transformation amounts to only 71%, whereas it is expected to reach an equilibrium value of 88% according to calculations with MTDATA®, and in qualitative agreement with microscopy. Apparently, although equation (7) can qualitatively describe the field dependence of the magnetization, it fails to

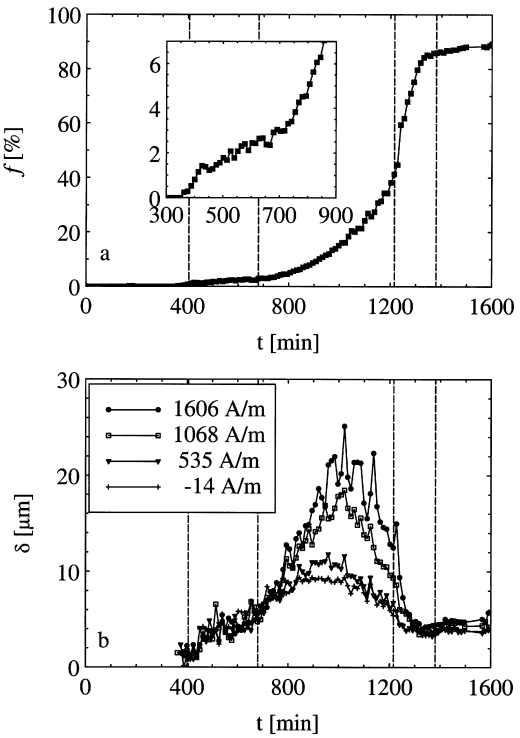

Fig. 4. The ferrite fraction f (a) and the mean grain radius δ (b) of C60 steel as a function of time for different applied magnetic fields.

describe the observed approach to saturation at the highest magnetic fields and underestimates the saturation rotation of the polarization φ_s. In order to obtain the correct final ferrite fraction, the reduced magnetization $m(H)$ obtained from the fitting procedure is reduced by a factor 0.80 throughout the measurement. This adjusted value of $m(H)$ is applied in the further analysis of the experiment. In this procedure we have assumed that the actual reduced magnetization shows the same relative variations as the calculated reduced magnetization during all stages of the transformation.

The resulting ferrite fraction as a function of time is shown in Fig. 4(a). At the onset of the pearlite formation ($t = 700$ min) the pro-eutectoid ferrite fraction is 3%, which is comparable with the pro-eutectoid ferrite formed in a previous continuous cooling experiment [2]. The ferrite fraction continues to increase until about $t = 1350$ min where it levels off, signaling the end of the phase transformation.

The mean ferrite grain radius δ is shown in Fig. 4(b) at different values of the applied magnetic field as a function of time and in Fig. 5 as a function of the applied magnetic field for the same stages of the transformation as in Fig. 2. These figures show that before the onset of the pearlite formation and after the completion of the transformation, there is a relatively weak dependence of δ on the applied magnetic field. These regions correspond to high values for $m(H = 1650$ A/m). However, in the intermediate range, where the pearlite formation takes place, there is a relatively strong field dependence of the mean grain size δ. At high magnetic fields δ is twice as large as at low fields. Furthermore, a distinct peak in δ occurs in Fig. 4(b) during the early stages of the pearlite formation. The maximum of the peak at $t = 1000$ min coincides with a ferrite fraction of 16%, and its height is distinctly field dependent. The mean grain radius of pro-eutectoid ferrite just before the onset of the pearlite formation reached 7 μm, while at the end of the transformation δ drops to about 5 μm.

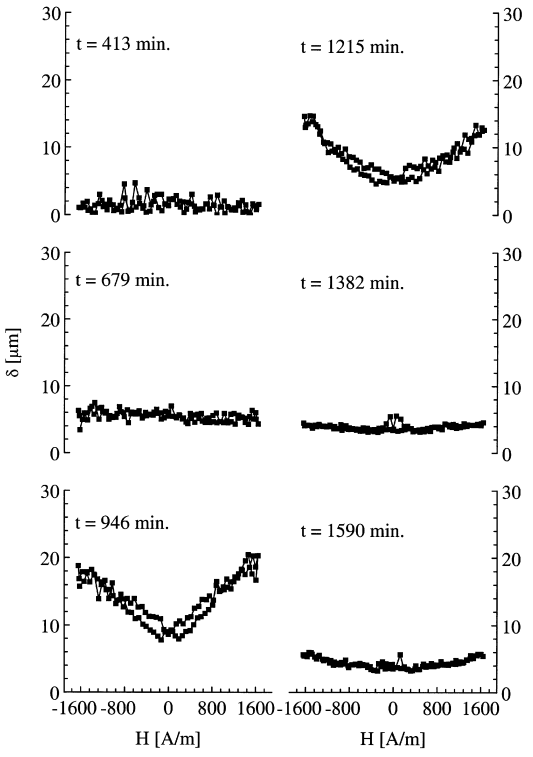

Fig. 5. The mean grain radius δ of C60 steel as a function of the applied field at different stages during the transformation.

The origin of the field dependence of the mean grain radius δ is most likely the presence of multi-domain grains in combination with variations in the effective thickness of the sample. In an applied magnetic field, the domain walls move when the applied magnetic field varies. The domain walls never completely disappear, because the applied magnetic field is not sufficiently large to obtain single-domain ferrite grains. Why this effect only takes place during the early stages of the pearlite formation, and not towards the end, is not clear. It is possible that in the final stages of the transformation, the high pearlite fraction and the decrease in the interlamellar spacing in the pearlite introduce a significant increase in the density of domain wall pinning sites, which halts the domain wall movement. This is consistent with the observed increase in H_c.

Figure 4(b) shows that during the formation of pro-eutectoid ferrite and during the early stages of the pearlite formation ($t \leq 750$ min), the mean grain radius increases almost linearly with time at a rate of 1 μm/h ($\approx 3^{\circ}A/s$). A comparison of the ferrite fraction with the mean grain volume, calculated from the mean grain radius, shows that the ferrite grain density during these stages of the transformation amounts to $2 \times 10^{13}/m^3$. This means that, assuming an austenite grain diameter of 50 μm, on average two ferrite grains form per austenite grain, which is comparable with the results presented by van Leeuwen *et al.* [24] for low-carbon steels at low cooling rates.

4. CONTINUOUS COOLING EXPERIMENTS ON C35 STEEL

4.1. Experiment

We have also performed neutron depolarization experiments on the phase transformation in C35 steel during continuous cooling. The composition of the C35 steel sample, as determined by infrared absorption spectrometry and X-ray fluorescence, is given in Table 1. The equilibrium transformation temperatures for the composition of the C35 steel were evaluated with MTDATA® and amount to $A_3 = 1055$ K for the austenite–ferrite transform-

ation, $A_1^+ = 994$ K and $A_1^- = 965$ K for the pearlite formation.

The applied magnetic field H was varied between 825 and -825 A/m. The varying magnetic field was applied as a "saw-toothed" function with a period of 1 s, which was divided into 50 time channels, in order to measure the depolarization matrix for 50 different magnetic field values. The measurement lasted 60 s for each element of the depolarization matrix. The ring-shaped sample was polished to a thickness of 0.30 mm, heated to a temperature of 1148 K and annealed for 90 min. After this annealing in the single-phase γ region, the samples were cooled at a constant rate of 9.7 K/h.

After completing the experiment and cooling to room temperature, a micrograph of the final microstructure of the sample was made, which showed that both the pro-eutectoid ferrite and the pearlite have formed in bands, oriented along the rolling direction. This texture is the result of an inhomogeneous distribution of Mn, created during hot rolling. In the experiment the transmission direction of the neutron beam is oriented along the rolling bands. A quantitative image analysis of the micrograph reveals that the fraction of pro-eutectoid ferrite is 42%, while the total fraction of ferrite is 93%. The mean ferrite radius of pro-eutectoid ferrite is 12.9 μm, while that of the pearlite regions is 13.6 μm. The average distance between the rolling bands is 29 μm.

4.2. Results and discussion

The A_3-temperature of the C35 steel is 1055 K according to the MTDATA® calculations, which is about 10 K higher than T_C. This means that during a relatively slow cooling experiment, the transformation from austenite to ferrite could start above T_C. Therefore, upon reaching T_C, below which neutron depolarization becomes sensitive to the formation of ferrite, part of the transformation could already have taken place. If this is the case, the rotation of the polarization vector φ will rapidly increase just below T_C to a value proportional to $\mu_0 M_s$ and the formed ferrite fraction.

The rotation determined from the depolarization matrix at the highest magnetic field is shown in Fig. 6. The rotation becomes non-zero at T_C (= 1043 K), but does not show a rapid increase, indicating that only a small ferrite fraction has formed above T_C. At $T = 970$ K the formation of pearlite starts, indicated by a rapid increase in the rotation during the transformation of austenite to pearlite. The field-dependent rotation φ is given in Fig. 7 for six different temperatures during the experiment. Each curve represents a full hysteresis loop for the magnetization. We have applied the same quantitative analysis of the measured magnetization curves as was used for the experiments on C60 steel (see Section 3).

First, the coercive field H_c was determined. As shown in Fig. 8(a), the coercive field increases gradually in value with increasing pro-eutectoid ferrite fraction during cooling. During the formation of pearlite H_c increases rapidly from 40 to 135 A/m. The coercive field during the formation of pro-eutectoid ferrite is similar in value to the coercive field determined for C60 steel. However, the coercive field at the end of the pearlite formation is

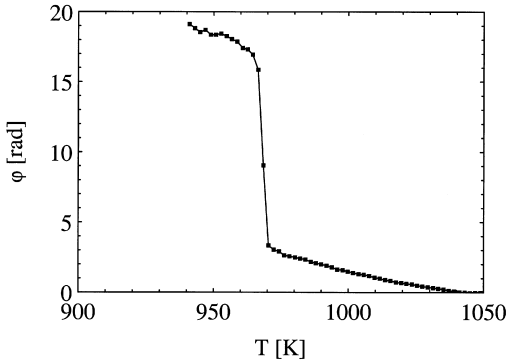

Fig. 6. The rotation of the polarization vector φ as a function of temperature during continuous cooling of C35 steel at the maximum applied magnetic field of $H = 825$ A/m.

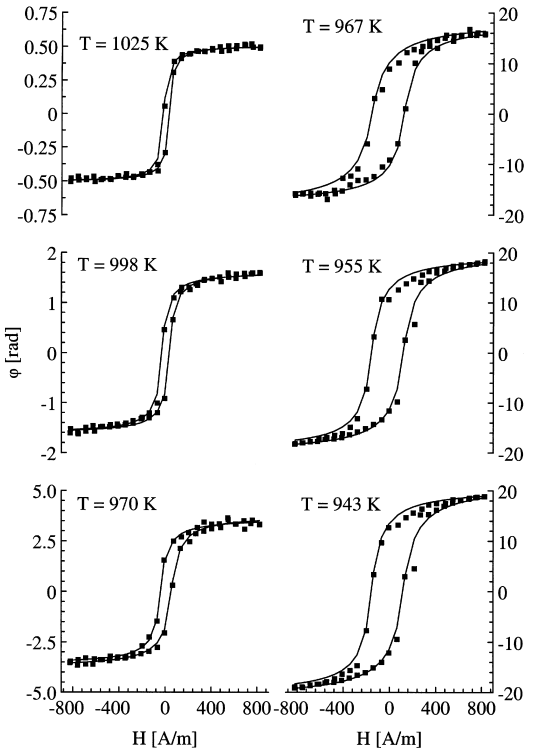

Fig. 7. The rotation of the polarization vector φ as a function of the applied field at different stages during the transformation of C35 steel. The data points give the measurements, while the solid lines are the results of the fit with equation (7).

higher than for C60 steel. Generally, H_c increases with the fraction of pearlite [14], and therefore it would be expected that C60 steel has a higher H_c than C35 steel. However, the micrographs of the fully transformed samples reveal that in the C60 sample partial spheroidizing of cementite has taken place, and that the pearlite lamella spacing is larger than for C35. Since pinning of the domain walls by the cementite lamellae is one of the main causes of coercivity, the difference in the pearlite microstructures between the samples is at the origin of the difference in H_c at the end of the transformation.

Further quantitative analysis of each measured magnetization curve consisted of fitting the curves to the field-dependent magnetization [21, 22] given by equation (7). With these fits (see Fig. 7), the reduced magnetization $m(H = 825\ \text{A/m})$ was determined, which is given as a function of temperature in Fig. 8(b). The value of the reduced magnetization at the highest applied magnetic field $m(H = 825\ \text{A/m})$ decreases with increasing pro-eutectoid fraction and decreasing temperature. At the start of the pearlite transformation m shows a sizable reduction. In contrast to the experiment on C60 steel, the transformation of austenite to pearlite takes place during the measurement of only a few depolarization matrices. Because the sample is rapidly changing during the measurement of these matrices, there is limited accuracy in the parameters derived in this range of the experiment. The minimum in m during the pearlite formation in the experiment on C60 is not observed for C35. The value of $m(H = 825\ \text{A/m})$ at the end of the experiment on C35 is smaller than the value of $m(H = 1650\ \text{A/m})$ found for C60, which is partially due to the lower maximum applied magnetic field during the C35 experiment. However, it could also be the result of the difference in the pearlite microstructures in both samples. If the fitted values of $m(H)$ are used to calculate the ferrite fraction, the fraction at the end of the transformation is too small (79%), while quantitative microscopy on the sample shows that a fraction of 93% is reached. To get the correct final ferrite fraction, the same procedure as used for C60 is performed and the fitted values of $m(H)$ are multiplied with a factor 0.85.

The ferrite fraction is given in Fig. 9(a) and shows an increase at a constant rate until the transformation to pearlite starts. At the onset of the pearlite formation a pro-eutectoid ferrite fraction of 16% is reached, which is considerably smaller than the fractions determined by microscopy (42%), and predicted by MTDATA® (47%). The mean grain radius determined at $H = 825\ \text{A/m}$ is shown in Fig. 9(b) and indicates that the growth rate starts to decrease as the transformation progresses. The mean grain radius reaches a value of 20 μm before

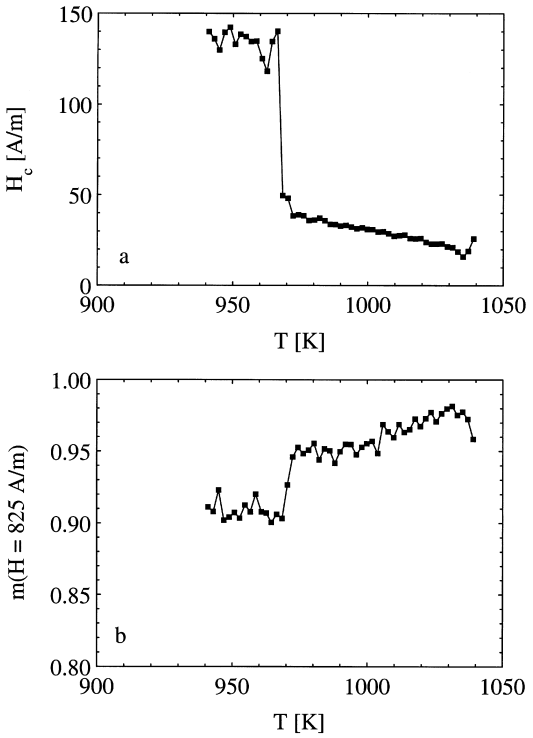

Fig. 8. The coercive magnetic field H_c (a) and the reduced magnetization at the highest applied magnetic field $m(H = 825\ \text{A/m})$ (b) for C35 steel as a function of temperature, determined by fitting the magnetization curves with equation (7).

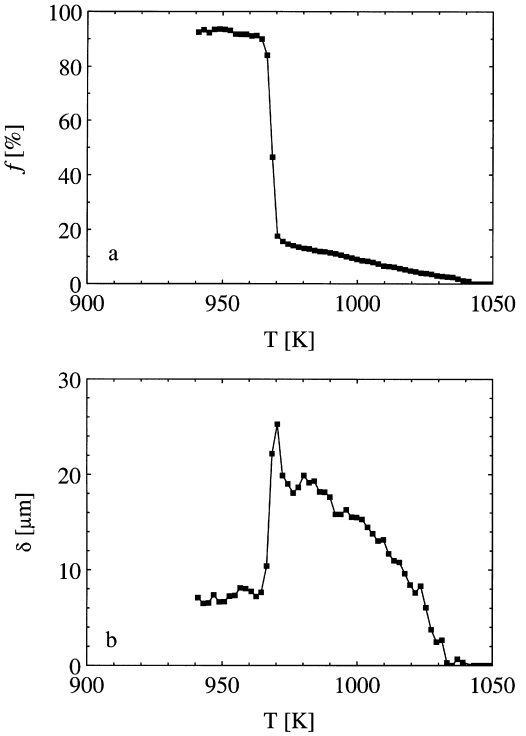

Fig. 9. The ferrite fraction f (a) and the mean grain radius δ (b) as a function of temperature during continuous cooling of C35 steel at the maximum applied magnetic field of $H = 825\ \text{A/m}$.

the onset of the pearlite formation, which is larger than the value found by microscopy (12.9 μm). As before, the early stages of the pearlite formation coincide with a peak in δ. After the peak, δ drops to 7 μm.

The mean grain radius as a function of the applied magnetic field is given in Fig. 10. During the first ($T = 1025$ K) and final ($T \lesssim 967$ K) stages of the experiment, there is little or no field dependence of the mean grain radius. However, starting at $T \approx 1018$ K and persisting until the end of the pearlite formation, there is a significant field dependence, which is most pronounced during the peak in δ at $T = 970$ K. In the analysis of C60 it was observed that this field dependence coincided with the formation of pearlite, but in this experiment the field dependence starts around 1018 K, while the pearlite formation only starts after cooling below 970 K. For both steels the field dependence of δ is observed when the mean grain radius at the highest applied field is 810 μm. These results suggest that in ferrite grains of this magnitude multiple magnetic domains can form when the applied field is not large enough to form single domain particles. The variation in the grain radius δ with applied magnetic field is then the result of the movement of the domain walls within these grains, in combination with variations in the effective thickness of the sample, as was suggested earlier for the experiments on C60.

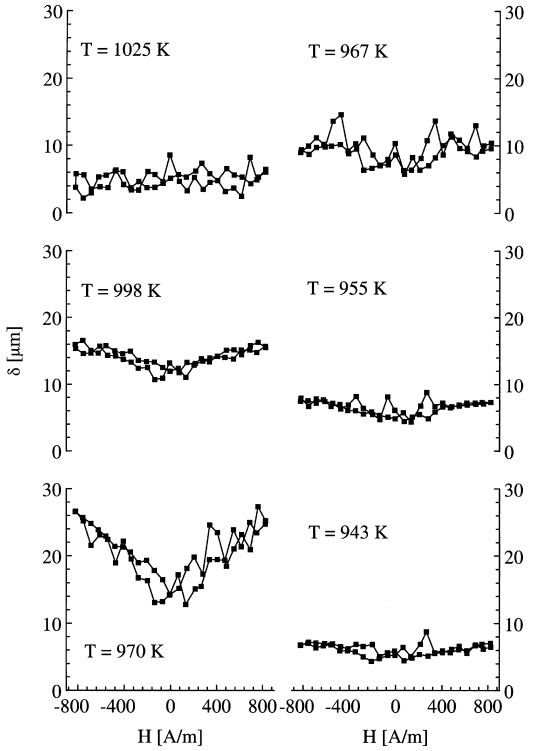

Fig. 10. The mean grain radius δ of C35 steel as a function of the applied magnetic field at different stages of the transformation.

5. CONCLUSIONS

We have performed neutron depolarization experiments on the ferrite formation in the medium-carbon steels C60 and C35 in a varying applied magnetic field. The continuous measurements of the hysteresis curves of the magnetization give essential information on the microstructure of the ferromagnetic ferrite grains. During the austenite–ferrite phase transformation the coercive magnetic field H_c and the reduced magnetization m do not significantly change. The start of the pearlite formation is indicated by a strong increase of H_c and a decrease of m. The increase in H_c signals a pinning of magnetic domain walls in the pearlite phase, which is sensitive to the pearlite microstructure, while the decrease in m indicates multi-domain behavior in the pearlite colonies. When the pearlite formation is complete, H_c saturates at a constant value, while m strongly varies at the transformation and assumes a relatively high value at the end of the pearlite formation. Using the relative variation of m during the transformation, the ferrite fraction and the mean particle size were evaluated. The field dependence of the mean particle size during the pearlite formation is a strong indication of multi-domain behavior, which is weak in the austenite–ferrite transformation and at the end of the pearlite formation.

Acknowledgements—The Netherlands Foundation of Technical Sciences (STW) is thanked for financial support.

REFERENCES

1. Krielaart, G. P., Rekveldt, M. Th., Brakman, C. M. and van der Zwaag, S., *Z. Metallk.*, 1994, **85**, 709.
2. te Velthuis, S. G. E., Rekveldt, M. Th. and van der Zwaag, S., *Ironmaking & Steelmaking*, 1995, **22**, 81.
3. te Velthuis, S. G. E., Rekveldt, M. Th., Sietsma, J. and van der Zwaag, S., *Physica B*, 1997, **234–236**, 1027.
4. te Velthuis, S. G. E., Rekveldt, M. Th., Sietsma, J. and van der Zwaag, S., *Physica B*, 1998, **241–243**, 1234.
5. Halpern, O. and Holstein, T., *Phys. Rev.*, 1940, **59**, 960.
6. Rekveldt, M. Th., *Z. Phys.*, 1973, **259**, 391.
7. Rosman, R. and Rekveldt, M. Th., *J. Magn. Magn. Mater.*, 1991, **95**, 319.
8. Stüsser, N., Rekveldt, M. Th. and Spruijt, T., *Phys. Rev.*, 1985, **B31**, 5905.
9. te Velthuis, S. G. E., Ph.D. thesis, Delft University of Technology, 1999.
10. Rekveldt, M. Th., *J. Magn. Magn. Mater.*, 1976, **1**, 344.
11. Jiles, D. and Atherton, D., *J. Magn. Magn. Mater.*, 1986, **61**, 48.
12. Jiles, D., *Introduction to Magnetism and Magnetic Materials*. Chapman & Hall, London, 1991.
13. Bozorth, R., *J. appl. Phys.*, 1937, **8**, 575.
14. Hetherington, M., Jakubovics, J., Szpunar, J. and Tanner, B., *Phil. Mag. B*, 1987, **56**, 561.

15. Beale, A., Hetherington, M., Jakubovics, J., Lewis, B. and Scruby, C., *Mater. Res. Soc. Symp. Proc.*, 1991, **232**, 313.
16. Wafik, A. and Razik, N., *Physica status solidi (a)*, 1991, **126**, 451.
17. Swisher, J., English, A. and Stoffers, R., *Trans. Am. Soc. Metals*, 1969, **62**, 257.
18. English, A., *Acta metall.*, 1967, **15**, 1573.
19. Jiles, D., *J. appl. Phys.*, 1988, **63**, 2980.
20. Stoner, F. E. C. and Wohlfahrt, E., *Phil. Trans. R. Soc. Lond. A*, 1948, **240**, 599.
21. Frölich, O., *Electrotech. Z.*, 1881, **2**, 134.
22. Kennelly, A., *Trans. Am. Inst. elect. Engrs*, 1891, **8**, 485.
23. Iványi, A., *Hysteresis Models in Electromagnetic Computation*. Akadémiai Kiadó, Budapest, 1997.
24. van Leeuwen, Y., Kop, T. A., Sietsma, J. and van der Zwaag, S., *Proceedings 3rd European Mechanics of Materials Conference on Mechanics and Multi-Physics Processes in Solids: Experiments, Modeling, Applications (Euromech–Mecamat–EMMC3)*, Oxford, 23–25 November 1998.